JSHC
Japan Society of
Histochemistry and Cytochemistry
Established 1959

Acta Histochem. Cytochem. 48 (2): 27–36, 2015
doi: 10.1267/ahc.14068

# Immunohistochemical and Morphofunctional Studies of Skeletal Muscle Tissues with Electric Nerve Stimulation by *In Vivo* Cryotechnique

**Yuki Fukasawa[1], Nobuhiko Ohno[1], Yurika Saitoh[1], Takeshi Saigusa[2], Jun Arita[2] and Shinichi Ohno[1]**

*[1]Department of Anatomy and Molecular Histology, Interdisciplinary Graduate School of Medicine and Engineering, University of Yamanashi and [2]First Department of Physiology, Interdisciplinary Graduate School of Medicine and Engineering, University of Yamanashi, 1110 Shimokato, Chuo-city, Yamanashi 409–3898, Japan*

Received December 26, 2014; accepted March 3, 2015; published online April 16, 2015

In this study, morphological and immunohistochemical alterations of skeletal muscle tissues during persistent contraction were examined by *in vivo* cryotechnique (IVCT). Contraction of gastrocnemius muscles was induced by sciatic nerve stimulation. The IVCT was performed immediately, 3 min or 10 min after the stimulation start. Prominent ripples of muscle fibers or wavy deformation of sarcolemma were detected immediately after the stimulation, but they gradually diminished to normal levels during the stimulation. The relative ratio of sarcomere and A band lengths was the highest in the control group, but it immediately decreased to the lowest level and then gradually recovered at 3 min or 10 min. Although histochemical intensity of PAS reaction was almost homogeneous in muscle tissues of the control group or immediately after the stimulation, it decreased at 3 min or 10 min. Serum albumin was immunolocalized as dot-like patterns within some muscle fibers at 3 min stimulation. These patterns became more prominent at 10 min, and the dots got larger and saccular in some sarcoplasmic regions. However, IgG1 and IgM were immunolocalized in blood vessels under nerve stimulation conditions. Therefore, IVCT was useful to capture the morphofunctional and metabolic changes of heterogeneous muscle fibers during the persistent contraction.

**Key words:** cryotechnique, muscle contraction, nerve stimulation, serum proteins, glycogen

## I. Introduction

Common muscle fatigue usually involves progressive decline of performance during intensive muscle usage, resulting in reduced maximum muscle tension, decreased contraction speed and extension of relaxation time [5, 6]. Such muscle fatigue is reported to be caused by multiple physiological mechanisms, which are broadly divided into central and peripheral factors [14, 23]. Moreover, the main factors closely relating to functional impairment of muscle tissues are further classified into several peripheral factors, and previous studies have suggested the functional significance of structural, metabolic and electrophysiological changes induced during muscle fatigue [6]. However, previous morphological and histochemical studies for examining the muscle fatigue in living animal organs always required tissue resection or transvascular perfusion-fixation, which is affected by ischemia/anoxia or perfusion pressure. Such artificial modification during the common preparation steps may have some unintended effects on the obtained findings about the dynamic and progressive muscle nature of fatigue, so improved morphological preparation methods of muscle tissues without such technical artifacts would be necessary for *in vivo* analyses of muscle fatigue.

The "*in vivo* cryotechnique" (IVCT) is a relatively new tissue preparation method for many organs of living animals. By this approach, surgically exposed target organs of living animals are directly cryofixed with liquid

Correspondence to: Shinichi Ohno, M.D., Ph.D., Professor, Department of Anatomy and Molecular Histology, Interdisciplinary Graduate School of Medicine and Engineering, University of Yamanashi, 1110 Shimokato, Chuo-city, Yamanashi 409–3898, Japan. E-mail: sohno@yamanashi.ac.jp

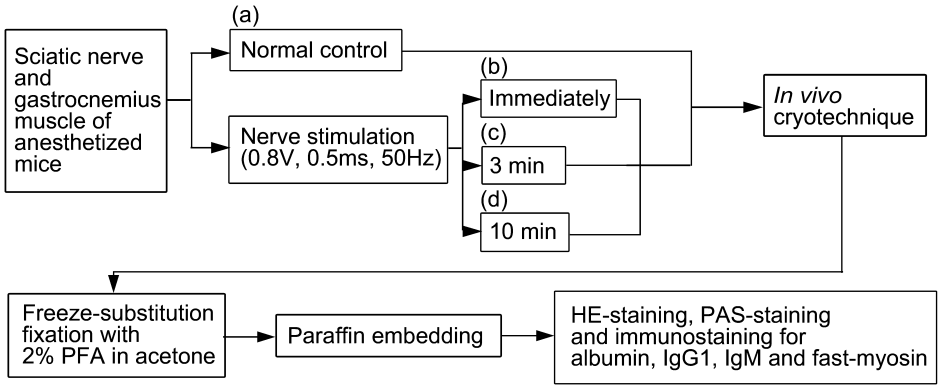


**Fig. 1.** A flow chart showing the experimental design of the present study. Mouse gastrocnemius muscles and sciatic nerves are exposed under anesthesia, and the *in vivo* cryotechnique (IVCT) is performed for normal mice (**a**) after the organ exposure *in vivo*. It is also performed immediately (**b**) after the nerve stimulation has started, or at 3 min (**c**) or 10 min (**d**) after the same stimulation. Following the IVCT, the frozen muscle tissues are freeze-substituted in acetone containing 2% paraformaldehyde (PFA) and embedded in paraffin wax. The deparaffinized thin sections are first stained with hematoxylin-eosin (HE) or periodic-acid-Schiff (PAS), and then immunostained for albumin, IgG1, IgM and fast-myosin.

isopentane-propane cryogen (−193°C) without tissue resection or perfusion-fixation [20]. Therefore, it is now known to be a unique and innovative method with some technical merits that overcome the previous artifact problems, such as loss of blood supply or artificial perfusion pressure, during the preparation steps. For the past twenty years, it has been applied to various tissues and organs of living animals to detect dynamic alterations of tissue morphology or signaling molecules, and also to preserve soluble components in various cells and tissues *in situ* [16, 18, 19, 29]. In particular, it has also become a powerful tool to observe the intracellular distributions of soluble glycogen particles and the immunolocalizations of small serum proteins [12, 17]. Therefore, it was suggested that IVCT would be useful to examine the dynamically changing skeletal muscle tissues, and reveal metabolic or molecular alterations in contracting muscle fibers of living animals. In the present study, we morphofunctionally and immunohistochemically examined living mouse gastrocnemius muscle tissues prepared using IVCT, and mainly focused on their morphological alteration, metabolic glycogen consumption and immunohistochemical changes of serum proteins under persistent skeletal muscle contractions with sciatic nerve stimulation.

## II. Materials and Methods

### *Experimental design of muscle contraction with nerve stimulation*

The present animal experiment was approved by the University of Yamanashi Animal Care and Use Committee. Twelve experimental male ICR mice, aged 8 weeks, in addition to thirty-two mice for the preliminary study, were purchased from Japan SLC (Shizuoka, Japan) and housed under ad libitum access to food and water. Their gastrocnemius muscle specimens were prepared as described below (Figs. 1, 2a). Briefly, both gastrocnemius muscles and sciatic nerves of mice were exposed under anesthesia with sodium pentobarbital. For experimental electric stimulation, the exposed sciatic nerves were gently mounted on a set of two handmade tungsten hooks, which were connected to bipolar electrodes, resulting in their isolation from adjacent organ tissues (Fig. 3a). Conventional electric stimulation was continuously performed with pulses lasting 0.5 ms at a voltage of 0.8 V and frequency of 50 Hz for the following time intervals. In some mice, their Achilles tendons were cut and connected to a tension monitor with strings, and then the time-lapse changes of such tension were continuously monitored (Figs. 3b, 4a), in addition to various stimulation voltages required for the maximal contraction. The stimulation voltage was most effective at about 0.4 V for maximal contraction, so the final stimulation voltage was set to be constant at 0.8 V for the muscle preparation without further tension measurement.

### *Subsequent tissue preparation steps using IVCT*

The mice used for morphofunctional analyses were divided into four experimental groups. (a) A control group: the exposed gastrocnemius muscles were directly cryofixed without nerve stimulation (Figs. 1a, 2). (b)–(d) Electric stimulation groups: they were similarly cryofixed immediately (b), 3 min (c) or 10 min (d) after the start of electric stimulation of sciatic nerves, resulting in persistent contraction of the gastrocnemius muscle (Figs. 1b–d, 3, 4). In stimulation groups (c) and (d), just before the IVCT, the electric stimulation was temporarily stopped for a few seconds to relax the gastrocnemius muscle and confirm its contraction. During the nerve stimulation period, the exposed sciatic nerves and gastrocnemius muscles were carefully protected from air-drying by covering with a piece of moist filter paper containing physiological saline. Then, the IVCT was routinely performed for each experimental group (Fig. 3a, b), as described previously [25]. Briefly, liquid isopentane-propane cryogen (−193°C) was prepared in advance by bubbling propane gas in liquid isopentane cooled in liquid nitrogen (−196°C), which was then poured over the gastrocnemius muscles of anesthetized mice (Figs. 2a, 3a).

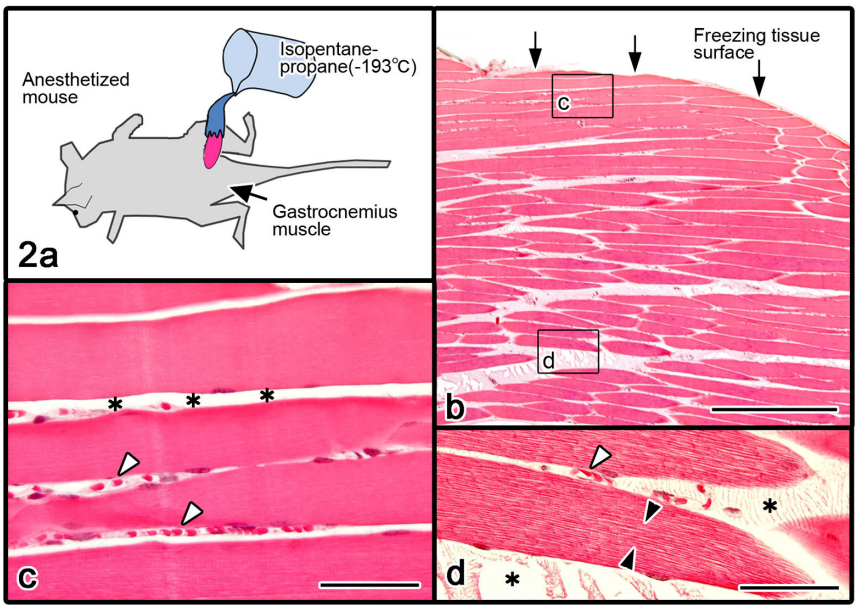


**Fig. 2.** (**a**) A schematic drawing showing how to perform IVCT for living mouse gastrocnemius muscles. The gastrocnemius muscle of the anesthetized mouse is exposed and cryofixed by pouring liquid isopentane-propane cryogen (−193°C) precooled in liquid nitrogen onto it. (**b–d**) Light micrographs of thin tissue sections prepared by IVCT and stained with HE. At low magnification (**b**), the gastrocnemius muscle is cryofixed from the freezing tissue surface (black arrows) into the deeper tissue areas. At higher magnification, there are no detectable ice crystals near the freezing tissue surface (**c**), and many open blood vessels, containing flowing erythrocytes (**c**; white arrowheads). However, many tiny ice crystals are observed as white empty spaces in the deep areas of muscle fiber tissues (**d**; black arrowheads). There are no ice crystals in the extracellular matrix near the tissue surface (**c**; asterisks), but large ice crystals are formed and clearly seen in the deep tissue areas (**d**; asterisks). Tissue areas marked with rectangles in (**b**) are highly magnified in (**c**) and (**d**). Bars=500 μm (**a**), 100 μm (**c, d**).

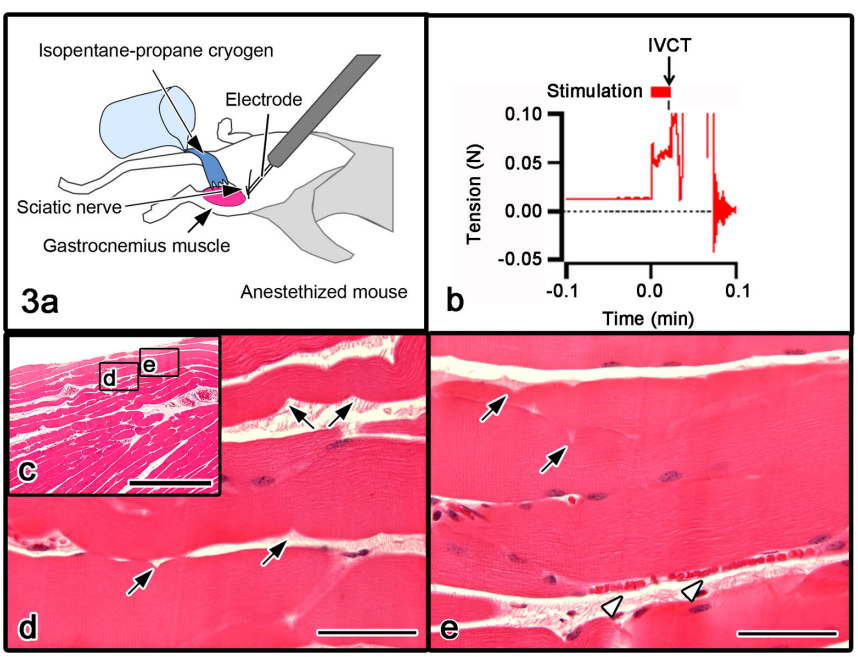


**Fig. 3.** (**a**) A schematic drawing showing how to stimulate a sciatic nerve of the anesthetized mouse. Both the gastrocnemius muscle and the sciatic nerve are exposed, and the sciatic nerve fiber is gently mounted on a bipolar electrode and isolated from adjacent organ tissues. (**b**) A trace example of the tension monitor is shown after the continuous nerve stimulation has started (red bar). IVCT is immediately performed (upper black arrow) by directly pouring the isopentane-propane cryogen onto the contracting muscle tissues. (**c–e**) Light micrographs of HE staining on thin sections of the muscle tissues prepared by IVCT immediately after the nerve stimulation has started. Ripples of muscle fibers (**d**; black arrows) and congestion of erythrocytes in blood vessels (**e**; white arrowheads) are clearly observed in the contracting muscle tissues. Tissue areas marked with rectangles in (**c**) are highly magnified in (**d**) and (**e**). Bars=100 μm, 500 μm (inset).

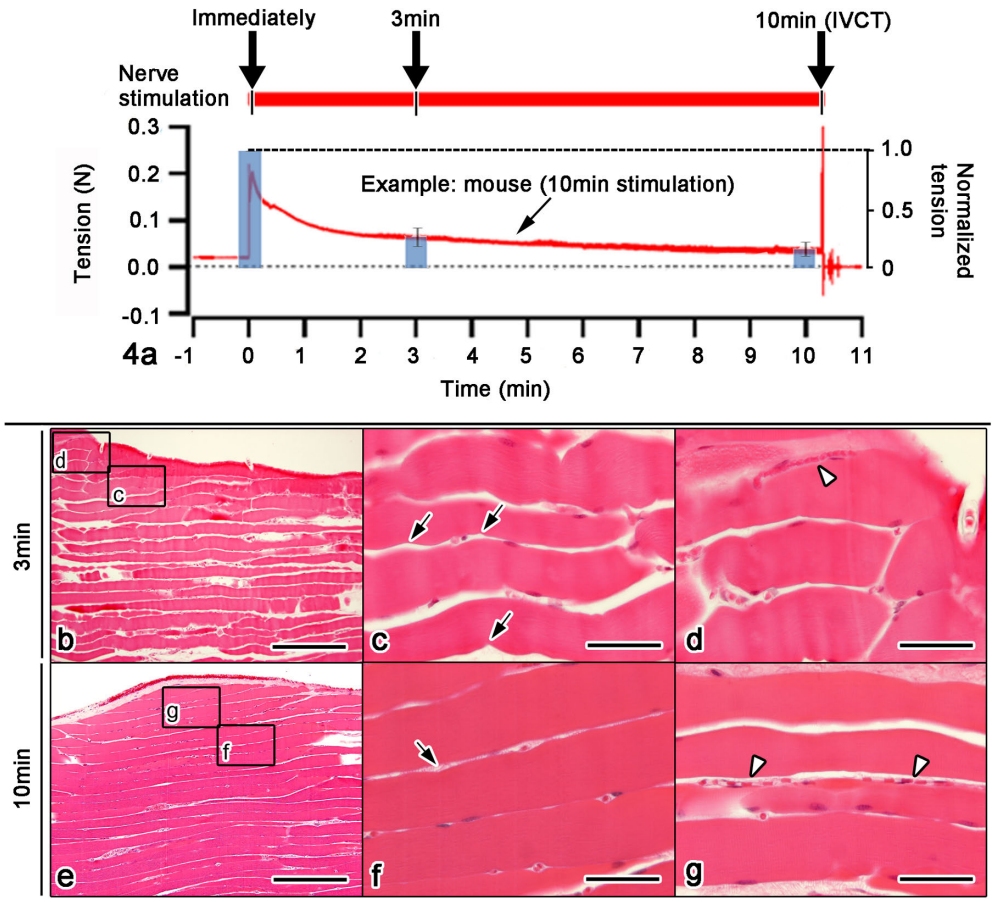


**Fig. 4.** (**a**) An example of the muscle tension curve obtained from a mouse gastrocnemius muscle during the sciatic nerve stimulation (upper red bar). A gradual decrease of the muscle tension is detected during the 10 min of nerve stimulation (**a**; red line). The timing of IVCT performance (upper black arrows) and the tension means of monitored mice (blue bar graph) are also shown in the graph. Light micrographs of HE staining on the thin section of gastrocnemius muscle tissues prepared by IVCT after 3 min (**b–d**) or 10 min (**e–g**) of the continuous nerve stimulation. Ripples of longitudinally cut muscle fibers (black arrows) and congestion of flowing erythrocytes in blood vessels (white arrowheads) are less prominent at 10 min of the nerve stimulation, compared with those at 3 min of the stimulation. Tissue areas marked with rectangles in (**b**) and (**e**) are highly magnified in (**c, d**) and (**f, g**) respectively. Bars=500 μm (**b, e**), 100 μm (**c, d, f, g**).

Practically, a little residual saline or blood on the tissue surface of the exposed muscles was gently removed with a piece of filter paper just before the IVCT. Then, the frozen muscles were removed in liquid nitrogen with a dental electric drill, as usual [25]. All cryofixed muscle specimens were routinely freeze-substituted in acetone containing 2% paraformaldehyde (PFA), and then embedded in paraffin wax.

### *Histochemistry of PAS and immunohistochemistry of serum proteins*

Thin paraffin sections cut to 3 μm thickness were mounted on glass slides (Matsunami Adhesive Slide, MAS; Matsunami Glass, Osaka, Japan). Some of them were routinely deparaffinized and stained with hematoxylin-eosin (HE) or periodic acid-Schiff (PAS). The other deparaffinized sections were rehydrated in phosphate-buffered saline (PBS) and immunostained for serum proteins by the avidin-biotin complex diaminobenzidine (ABC-DAB) method, as previously described with some modifications [17]. Briefly, the serial thin sections for immunoperoxidase-DAB staining were first treated with 1% hydrogen peroxide in PBS for the inhibition of endogenous peroxidase activity, and additionally incubated in 5% fish gelatin (Sigma, St. Louis, MO, USA). They were then incubated in primary antibodies at 4°C overnight, as described below, followed by corresponding secondary antibodies at room temperature for 2 hr. The primary antibodies were goat anti-mouse albumin, immunoglobulin G1 (IgG1) or IgM antibody (Bethyl Laboratories, Montgomery, TX, USA), and also mouse anti-fast myosin heavy chain antibody (Abcam, Tokyo, Japan). The secondary antibodies were the common biotinylated antibodies against goat or mouse IgG proteins (Vector Laboratories, Burlingame, CA, USA). The immunostained sections were then incubated with horseradish peroxidase (HRP)-conjugated avidin-biotin complex (ABC) for 1 hr (Vector Laboratories) and visualized with metal-enhanced 3,3'-diaminobenzidine (DAB) (ImmunoPure; Pierce Chemical, Rockford, IL) for 5 min. Finally, they were incubated in 0.04% osmium tetroxide solution for 5 min, and their light micrographs were taken using a light microscope (BX-61; Olympus, Tokyo, Japan).

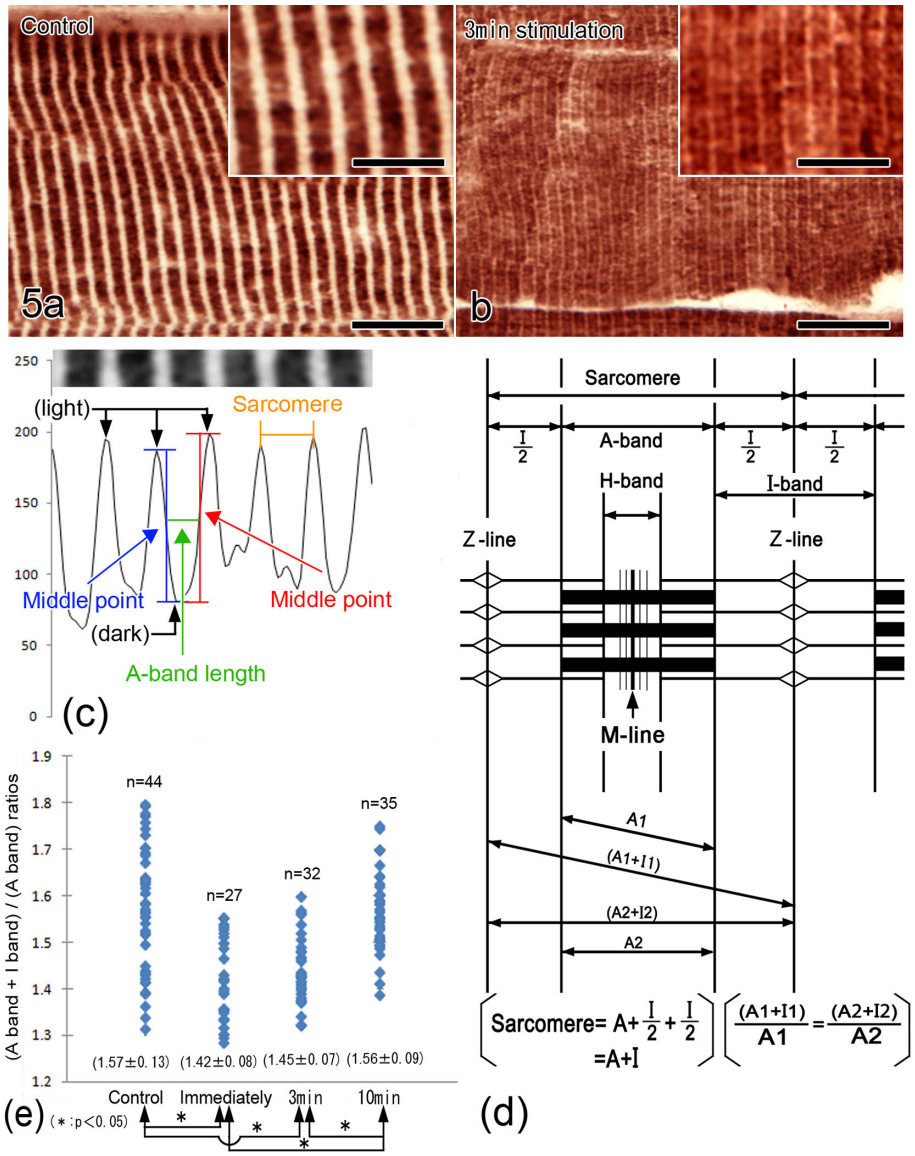


**Fig. 5.** (**a, b**) Light micrographs of fast-myosin immunostaining in mouse gastrocnemius muscle tissues prepared by IVCT without the nerve stimulation (**a**; control) or at 3 min after the start of stimulation (**b**). The lengths of sarcomeres with or without the nerve stimulation appear to be different between the two groups. Both insets show highly magnified pictures. (**c, d**) The lengths of A band are measured on light micrographs of immunostained fast-myosin, which is needed for calculating the full-width at half-maximum values of each sarcomere. The length of sarcomere is measured as the distance between two adjacent peaks of fast-myosin immunoreactivity. (**e**) Scattered plot diagram of the ratios of (sarcomere length)/(A band length). The numerical values at the bottom show the means and standard deviations, and the asterisks show significant difference (Tukey's multiple comparisons test, $p<0.05$, n=27–44). Bars=50 µm, 25 µm (insets).

***Quantitative analyses of muscle tissues at various time intervals of nerve stimulation***

Light micrographs of thin sections immunostained for fast-myosin were changed into 8 bits by a personal computer (Fig. 5a–c). Longitudinally cut muscle fibers were randomly selected in the digital images (Fig. 5a, b), and the grayscale values of striation in the muscle fibers were measured along individual lines (Fig. 5c), which were parallel to their running directions and drawn on Fiji/ImageJ (http://fiji.sc/Fiji). Almost all muscle fibers with A bands were immunopositive for the fast-myosin protein, but immunonegative for the slow-myosin one (data not shown), confirming that the gastrocnemius muscle is rich in the fast muscle fibers [2, 8, 30]. The lengths of A band were measured as the full-width at half-maximum values of the fast-myosin immunostaining density (Fig. 5c). The lengths of sarcomere (A band + I band) were measured as distances between two adjacent peaks of fast-myosin immunoreactivity (Fig. 5c, d). For statistical comparisons of muscle contraction states, the measured lengths were not directly used, but the relative ratio of (sarcomere length)/(A band length) was used since it is relatively unaffected by tissue-cutting angles, as shown in the scheme (Fig. 5d). Five sets of the ratios were selected in each muscle fiber, and their median

was used as the representative value for the muscle fiber (Fig. 5e). In each group, 27–44 muscle fibers were randomly selected from 3 mice, and the statistical significance was examined using Tukey's multiple comparison test.

## III. Results

***Morphological analyses of skeletal muscles using IVCT***

To observe muscle morphology *in vivo* under resting states with normal blood circulation, IVCT was performed by directly pouring the isopentane-propane cryogen to the exposed gastrocnemius muscle tissues in the normal mice (Fig. 2a). Thin tissue sections of the gastrocnemius muscles prepared by IVCT were first examined using HE staining (Fig. 2b–d). At the surface areas of muscle tissues, which were directly contacted with the isopentane-propane cryogen (−193°C), longitudinally cut sections of the muscle fibers could be clearly observed without any visible ice crystals at low or high magnifications by light microscopy (Fig. 2b, c). Such well-frozen tissue areas with no detectable ice crystals were obtained in the tissue surface within 200–300 μm, containing flowing erythrocytes at higher magnification (Fig. 2c). However, in the deeper areas far from the frozen tissue surface, many tiny ice crystals were easily detected in all skeletal muscle fibers along with intravascular damaged erythrocytes, in addition to void spaces of large ice crystals in the extracellular matrix (Fig. 2d). All of the muscle tissues for the following examination were selected in the surface tissue areas without visible ice crystals at 300–400 μm from the freezing contact plane (Fig. 2b).

***Dynamic changes of functional muscle fibers by the nerve stimulation***

In order to examine morphofunctional changes of contracting skeletal muscles *in vivo*, we performed the IVCT for gastrocnemius muscles continuously contracting upon the sciatic nerve electric stimulation (Figs. 3a, 4a). The maximal contraction of gastrocnemius muscles was achieved by gradually increasing stimulation voltages and then monitoring the saturation of resultant muscle tensions in pilot experiments (data not shown). Immediately after the initiation of maximal contraction, prominent ripples of muscle fiber surface or a wavy appearance of their sarcolemma were clearly observed in the skeletal muscle tissues (Fig. 3d, e), including congestion of flowing erythrocytes in some blood vessels (Fig. 3e). When the electric nerve stimulation continued on each bundled muscle fascicle for 3 min or 10 min (Fig. 4), the monitored muscle tension gradually declined, depending on the nerve stimulation time (Fig. 4a). Such muscle tensions more rapidly declined during the time of 3 min after the electric nerve stimulation started, and became about 26% of the maximum tension (Fig. 4a). Furthermore, at 10 min after similar stimulation, the monitored muscle tension continuously declined and reached about 16% of the maximum tension. By the HE staining, morphological changes, such as ripples and a wavy appearance of sarcolemma, observed immediately after the start of maximal muscle contraction, became less obvious after the longer sciatic nerve stimulation (Fig. 4b–g). At 3 min of the nerve stimulation, the ripples of skeletal muscle fibers were less detected in most muscle tissues, but still observed in some muscle fibers (Fig. 4b–d). In addition, the apparently congested erythrocytes were also seen in some blood vessels (Fig. 4d). However, at 10 min of the nerve stimulation, such ripples of the muscle fibers were much less detected, and the congested erythrocytes disappeared in many blood vessels (Fig. 4e–g). To compare the muscle contraction levels between such experimental groups, the thin sections prepared using IVCT were immunostained for mouse fast-myosin protein to distinguish the lengths of A band, I band and sarcomere clearly in the light micrographs (Fig. 5a, b). The total sarcomere length was calculated as the sum of measured A band and I band lengths (Fig. 5c, d). The total length of A band is always constant, but the lengths of both sarcomere and I band usually decrease during muscle contraction [9]. Then, the (sarcomere length)/(A band length) ratios were compared between control and experimental groups (Fig. 5e), which were considered to be unaffected by the tilting angles of muscle fibers (Fig. 5d). The mean ratio was the highest in the control muscle fibers (mean±SD, 1.57±0.13), but significantly decreased immediately after the nerve stimulation (1.42±0.08) (Fig. 5e). The ratio was still maintained at a low level after 3 min of the continuous muscle contraction (1.45±0.07), but became higher after 10 min of the nerve stimulation (1.56±0.09) (Fig. 5e). These findings demonstrate that gastrocnemius muscle contraction easily induces both ripple-like alteration or wavy sarcolemma of the muscle fibers and functional congestion of blood circulation, and that such morphological changes gradually diminish during the continuous muscle contraction along with the reduced contracting forces.

***Histochemical detection of glycogen particles in contracting muscle fibers***

The IVCT can well maintain soluble glycogen particles in hepatocytes of living mouse livers during the tissue preparation steps, as reported previously [17, 24]. To address how the continuous muscle contraction affects the glycogen content and distribution in functioning skeletal muscle fibers, thin sections of gastrocnemius muscle tissues prepared by IVCT were histochemically stained by the PAS method (Fig. 6). In the control group and another experimental group subjected to immediate freezing after the nerve stimulation, most of the muscle fibers were well stained by the PAS method, probably showing glycogen particles, and their PAS reactivities generally did not differ among the control or contracting muscle fibers (Fig. 6a, b). By contrast, the PAS reactivities were detected at various levels in the muscle fibers at 3 min or 10 min after the continuous electric nerve stimulation (Fig. 6c, d). Interestingly,

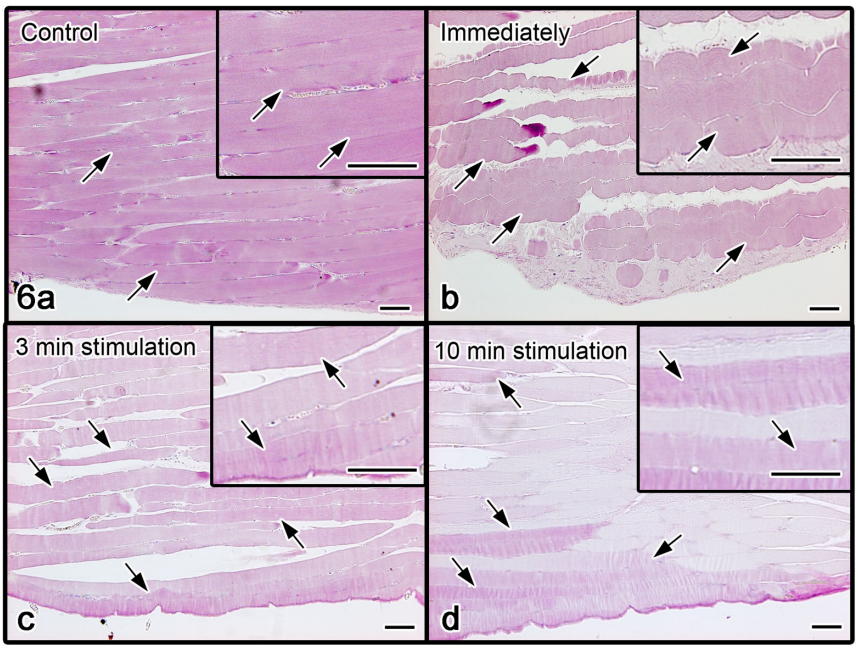


**Fig. 6.** Light micrographs of PAS staining in the mouse gastrocnemius muscle tissues prepared by IVCT without the nerve stimulation (**a**; control) or immediately (**b**), 3 min (**c**) or 10 min (**d**) after the stimulation has started. The PAS reactivities of muscle fibers are clearly seen in control (**a**; black arrows) and immediately after the stimulation (**b**; black arrows), but the PAS staining intensity becomes heterogeneous after 3 min and 10 min of the nerve stimulation (**c, d**; black arrows). Each inset is highly magnified. Bars=100 μm.

the muscle fibers with less intensive PAS staining were frequently localized in some areas of the deep muscle tissues. These findings suggest that the prolonged contraction of muscle fibers probably depletes glycogen particles in the skeletal muscle fibers, and their rapid consumption is relatively dependent on different regions of the muscle tissues.

***Immunolocalization of serum proteins in muscle fibers under contracting conditions***

We previously reported that functional cardiomyocytes of beating hearts in living mice have some intracellular albumin, presumably immunolocalized in T-tubules [27]. In addition, we also found that the loss of PAS reactivities from the cytoplasm was characteristic of damaged hepatocytes under mechanical or anoxic stress, which was accompanied by another type of cytoplasmic immunostaining of soluble serum proteins [24]. To address whether soluble serum proteins are distributed in the skeletal muscle tissues by the continuous muscle contraction, the serial sections prepared by IVCT were first stained with the common HE dyes, and then immunostained for serum albumin, IgG1 and IgM (Fig. 7). In the normal skeletal muscle tissues without nerve stimulation (Fig. 7a–e), all of albumin, IgG1 and IgM were restricted to the extracellular matrix and also within blood vessels. However, immediately after starting the continuous muscle contraction, the soluble albumin alone was found to be slightly immunolocalized as dot-like patterns within some muscle fibers (Fig. 7g, h). However, both IgG1 and IgM were immunolocalized in similar ways to those in the normal muscle tissues (Fig. 7d, e, i, j). At 3 min of the continuous muscle contraction, the dot-like immunoreaction products were more prominent in many muscle fibers (Fig. 7l, m). In addition, they were clearly seen in the muscle fibers after 10 min of the muscle contraction, and the total sizes of their immunoreaction dots became larger and appeared to be saccular in some regions of muscle fibers (Fig. 7q, r). By contrast, both IgG1 and IgM were still immunolocalized only within blood vessels in addition to the interstitium, but were not seen in the muscle fibers even after the continuous muscle contraction (Fig. 7n, o, s, t). The diffuse cytoplasmic immunostaining of these serum proteins, which had been frequently detected together with cellular damage or necrosis [17, 24], was not observed in the functioning skeletal muscle tissues, as revealed in the present study (Fig. 7). These findings demonstrate that soluble serum albumin in the extracellular matrix of skeletal muscle tissues easily enters the muscle fibers during the functional contraction of muscle fascicles, but their sarcolemmal permeability appeared to be unchanged even under the persistent muscle contraction.

## IV. Discussion

In the present study, the conventional IVCT was applied to gastrocnemius muscle tissues of living mice to examine their morphological changes and distribution of soluble serum proteins during continuous muscle contraction with sciatic nerve stimulation. As described above, the obtained results clearly demonstrate that the maximal muscle contraction induces some wavy structural changes of dynamic skeletal muscle fibers along with congestion of

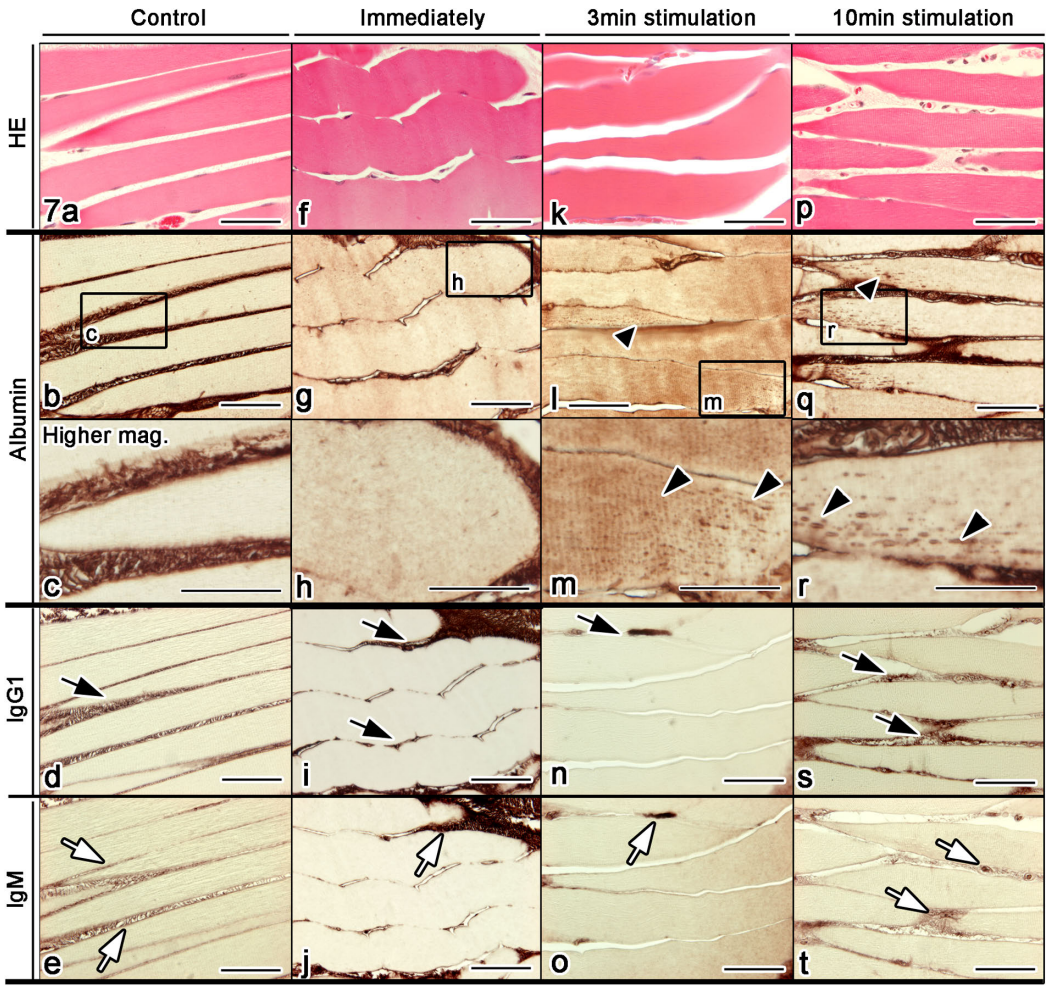


**Fig. 7.** Light micrographs of serial thin sections obtained from the mouse gastrocnemius muscle tissues, prepared by IVCT without the nerve stimulation (control; **a–e**), or immediately (immediately; **f–j**), 3 min (3 min stimulation; **k–o**) or 10 min (10 min stimulation; **p–t**) after the continuous nerve stimulation has started. The thin sections are stained with HE (**a, f, k, p**), and immunostained for albumin (**b, g, l, q**) (higher magnifications; **c, h, m, r**), immunoglobulin G1 (IgG1; **d, i, n, s**) or immunoglobulin M (IgM; **e, j, o, t**). Both IgG1 (**d, i, n, s**; black arrows) and IgM (**e, j, o, t**; white arrows) are immunolocalized in the extracellular matrix and blood vessels. In contrast, dot-like albumin immunostaining is observed in the sarcoplasm of contracting muscle fibers with the nerve stimulation (**l, m**; black arrowheads). The albumin immunoreaction products are more clearly detected after the longer nerve stimulation (**q, r**; black arrowheads). Tissue areas marked with rectangles in (**b**), (**g**), (**l**), (**q**) are highly magnified in (**c**), (**h**), (**m**), (**r**) respectively. Bars=50 μm.

erythrocytes in blood capillaries. The persistent muscle contraction with the gradual decrease of muscle tension also induced some reduction of PAS reactivity in the muscle fibers, which was accompanied by heterogeneous relaxation of muscle fibers and temporary relief of both wavy sarcolemma and erythrocyte congestion. Furthermore, soluble serum albumin, which was exclusively immunolocalized in the interstitium and also blood vessels under normal muscle conditions, appeared to enter the skeletal muscle fibers under the experimental contracting conditions. These findings demonstrate that the IVCT is highly useful to examine dynamic morphological changes and the distribution of soluble serum proteins in the functional muscle tissues during the prolonged contraction time, and suggest that these morphofunctional changes might be closely related to structural and metabolic adaptation of muscle fibers to the mechanical contraction.

We used a sustained contraction model rather than the more common tetanic contraction in the present study, in combination with IVCT. This protocol of experiments was based on our aim of examining the functional morphology of living mouse muscles under the maximal contraction conditions. Under the conventional tetanic stimulation, the muscle contraction and relaxation are repeated one after another in a short time interval. Therefore, it was technically difficult to perform reproducible cryofixation just at the muscle contraction period. By contrast, the sustained muscle contraction, which enabled the reproducible cryofixation of functioning gastrocnemius muscles contracted by the sciatic nerve stimulation, was considered to be an appropriate approach to examine histologically the contracting skeletal muscles by IVCT without the technical

artifacts that are always caused by the conventional tissue resection or perfusion-fixation. Since the tetanic muscle contraction model probably reflects more physiological muscle fatigue conditions *in vivo* [6], the further development of another suitable model in combination with IVCT is needed to examine the skeletal muscle tissues under such tetanic contraction of living mice.

The present application of IVCT to morphological analyses of skeletal muscle tissues has clearly demonstrated the congestion of erythrocytes usually flowing in blood vessels along with the decrease of sarcomere length of contracted muscle fibers. Such erythrocyte congestion has already been observed in other organs of living mice under abnormal conditions, where blood circulation was considered to be impaired, because of heart-arrest conditions [17, 28], ischemic model by blood vessel ligation [3] or thrombus formation by tumor cell metastasis [26]. It has been suggested that the blood flow into contracting muscle tissues is usually perturbed upon intensive muscle contraction, presumably due to the temporarily increased intramuscular pressure [1, 10]. The erythrocyte congestion observed in the present study could represent the impaired blood flow conditions into the contracting skeletal muscle tissues. This possibility is also supported by the relieved erythrocyte congestion after the prolonged muscle contraction, resulting in decreased tension of the muscle contraction, as shown in Figure 4.

The wave-like deformation of sarcolemma in the rippled muscle fibers rapidly appeared upon their contraction induced by the electric nerve stimulation, and time-dependently disappeared during the continuous muscle contraction with tension decrease. It should be noted that such sarcolemmal deformation was not prominent after 10 min of the long muscle contraction, as shown in Figure 4, while the muscle fascicles were still contracted, although the morphological contraction features were heterogeneously impaired in individual muscle fibers after 10 min of muscle contraction. One explanation for these findings is that the morphological deformation observed in each muscle fiber depended on its own contraction level, and the ripples of muscle fibers were caused by the decrease of muscle fiber length during the muscle contraction, which was disproportional to the size of their sarcolemma. Therefore, the redundant surface portions of sarcolemma may require wavy structures in order to be accommodated in the restricted muscle fiber length. A previous study has already revealed that the repeated contraction of muscle fibers could cause sarcolemmal damage, which was exacerbated in pathological states of muscle tissues, such as in Duchenne muscular dystrophy mice [22]. The substantial changes of abnormal sarcolemmal structures probably underlie the later sarcolemmal damage of muscle fibers, causing unusual passage of extracellular soluble proteins into the muscle fibers after the intensive muscle contraction [4, 13, 21].

In the present study, the gradually decreased levels of PAS reactivity for glycogen during the prolonged muscle contraction appeared to be heterogeneous in the gastrocnemius muscle *in vivo*, as revealed by IVCT. This is not due to the depth-dependent artifacts caused at the time of freezing, because the glycogen particles were much less extracted in these tissue areas at the time of freezing, and the PAS reaction was also evident even in the deeper areas. The heterogeneity of glycogen particles observed among the muscle fibers during the prolonged muscle contraction is not dependent on fast- or slow-twitch muscle fibers. This is because the immunostaining for fast- and slow-myosin proteins already revealed that all of the examined muscle fibers of mouse gastrocnemius muscles were fast-twitch muscle types, which were immunopositive only for the fast-myosin protein, not for the slow-myosin one (data not shown), which is consistent with previous studies [2, 8, 30]. It is well known that the muscle glycogen particles are rapidly utilized upon extensive muscle exercise, and the activity of the glycolytic enzyme system driven for glycogen breakdown is considered always to be affected by oxygen availability. Therefore, the lower oxygen availability could result in the more rapid consumption of glycogen particles in functioning muscle fibers [7], presumably due to the less effective production of ATP with anaerobic glycolysis through difficulties of functional respiration. This morpho-functional idea is now supported by our findings that the muscle contraction induced the prominent erythrocyte congestion at the first stage, indicating that oxygen delivery is perturbed within the contracting skeletal muscle tissues *in vivo*. The histochemical heterogeneity of PAS reaction products could be caused by topographically changing metabolic reactions in the muscle fibers near or far from the surface tissue of muscle fascicles *in vivo*.

As described in the present study using IVCT, there were no muscle fibers where soluble albumin diffusely entered the sarcoplasm under normal physiological conditions or even after the prolonged muscle contraction. However, the muscle contraction often produced dot-like immunoreaction products of soluble albumin in skeletal muscle fibers under the muscle contraction conditions. This contrasts with previous studies demonstrating that serum or extrinsic soluble molecules can diffusely enter the sarcoplasm upon extensive muscle contraction or even under normal physiological conditions [15, 22]. The IVCT has already been used to detect more detailed dynamic distributions of various intrinsic or extrinsic soluble molecules in living animal organs [20], showing the diffuse cytoplasmic immunostaining of serum proteins presumably due to their cell membrane damage [17, 24, 31]. As shown in Figure 7, the dynamic processes of muscle contraction probably did not disrupt the sarcolemmal integrity to allow the rapid influx of soluble serum proteins, such as albumin. In this context, the dot-like immunoreaction products of albumin in the skeletal muscle fibers may represent another translocation into some intracellular compartments in the functional muscle fibers. One possibility is that they might be T-tubules in the sarcoplasm because we have already reported

the similar dot-like patterns of the albumin immunolocalization in cardiomyocytes of actively beating heart tissues, as already revealed by IVCT [27]. In this regard, the saccular swelling of dot-like albumin immunostaining in muscle fibers after 10 min of muscle contraction may reflect swelling of T-tubules related to muscle fatigue [11]. Further morphofunctional studies at the electron microscopic level are now required to elucidate the more detailed albumin distribution and the functional significance of albumin translocation into the contracting muscle fibers.

## V. References


1. Barcroft, H. and Millen, J. L. (1939) The blood flow through muscle during sustained contraction. *J. Physiol.* 97; 17–31.
2. Burkholder, T. J., Fingado, B., Baron, S. and Lieber, R. L. (1994) Relationship between muscle fiber types and sizes and muscle architectural properties in the mouse hindlimb. *J. Morphol.* 221; 177–190.
3. Chen, J., Terada, N., Saitoh, Y., Huang, Z., Ohno, N. and Ohno, S. (2013) Detection of MAPK signal transduction proteins in an ischemia/reperfusion model of mouse intestine using in vivo cryotechnique. *Histochem. Cell Biol.* 140; 491–505.
4. Dudley, R. W., Danialou, G., Govindaraju, K., Lands, L., Eidelman, D. E. and Petrof, B. J. (2006) Sarcolemmal damage in dystrophin deficiency is modulated by synergistic interactions between mechanical and oxidative/nitrosative stresses. *Am. J. Pathol.* 168; 1276-87; 1404–1405.
5. Enoka, R. M. and Stuart, D. G. (1992) Neurobiology of muscle fatigue. *J. Appl. Physiol.* 72; 1631–1648.
6. Fitts, R. H. (1994) Cellular mechanisms of muscle fatigue. *Physiol. Rev.* 74; 49–94.
7. Gollnick, P. D., Karlsson, J., Piehl, K. and Saltin, B. (1974) Selective glycogen depletion in skeletal muscle fibres of man following sustained contractions. *J. Physiol.* 241; 59–67.
8. Hitomi, Y., Kizaki, T., Watanabe, S., Matsumura, G., Fujioka, Y., Haga, S., Izawa, T., Taniguchi, N. and Ohno, H. (2005) Seven skeletal muscles rich in slow muscle fibers may function to sustain neutral position in the rodent hindlimb. *Comp. Biochem. Physiol. B. Biochem. Mol. Biol.* 140; 45–50.
9. Huxley, A. F. and Niedergerke, R. (1954) Structural changes in muscle during contraction; interference microscopy of living muscle fibers. *Nature* 22; 971–973
10. Jarvholm, U., Styf, J., Suurkula, M. and Herberts, P. (1988) Intramuscular pressure and muscle blood flow in supraspinatus. *Eur. J. Appl. Physiol. Occup. Physiol.* 58; 219–224.
11. Krolenko, S. A. and Lucy, J. A. (2001) Reversible vacuolation of T-tubules in skeletal muscle: Mechanisms and implications for cell biology. *Int. Rev. Cytol.* 202; 243–298.
12. Li, Z., Ohno, N., Terada, N. and Ohno, S. (2006) Immunolocalization of serum proteins in living mouse glomeruli under various hemodynamic conditions by "in vivo cryotechnique". *Histochem. Cell Biol.* 126; 399–406.
13. Lynch, G. S., Rafael, J. A., Chamberlain, J. S. and Faulkner, J. A. (2000) Contraction-induced injury to single permeabilized muscle fibers from mdx, transgenic mdx, and control mice. *Am. J. Physiol. Cell Physiol.* 279; C1290–1294.
14. Maclaren, D. P., Gibson, H., Parry-Billings, M. and Edwards, R. H. (1989) A review of metabolic and physiological factors in fatigue. *Exerc. Sport Sci. Rev.* 17; 29–66.
15. McNeil, P. L. and Khakee, R. (1992) Disruptions of muscle fiber plasma membranes. Role in exercise-induced damage. *Am. J. Pathol.* 140; 1097–1109.
16. Ohno, N., Terada, N., Murata, S., Katoh, R. and Ohno, S. (2005) Application of cryotechniques with freeze-substitution for the immunohistochemical demonstration of intranuclear pCREB and chromosome territory. *J. Histochem. Cytochem.* 53; 55–62.
17. Ohno, N., Terada, N. and Ohno, S. (2006) Histochemical analyses of living mouse liver under different hemodynamic conditions by "in vivo cryotechnique". *Histochem. Cell Biol.* 126; 389–398.
18. Ohno, N., Terada, N., Saitoh, S., Zhou, H., Fujii, Y. and Ohno, S. (2007) Recent development of in vivo cryotechnique to cryobiopsy for living animals. *Histol. Histopathol.* 22; 1281–1290.
19. Ohno, S., Terada, N., Fujii, Y., Ueda, H. and Takayama, I. (1996) Dynamic structure of glomerular capillary loop as revealed by an in vivo cryotechnique. *Virchows Arch.* 427; 519–527.
20. Ohno, S., Terada, N., Ohno, N., Saitoh, S., Saitoh, Y. and Fujii, Y. (2010) Significance of 'in vivo cryotechnique' for morphofunctional analyses of living animal organs. *J. Electron Microsc. (Tokyo).* 59; 395–408.
21. Palacio, J., Galdiz, J. B., Alvarez, F. J., Orozco-Levi, M., Lloreta, J. and Gea, J. (2002) Procion orange tracer dye technique vs. identification of intrafibrillar fibronectin in the assessment of sarcolemmal damage. *Eur. J. Clin. Invest.* 32; 443–447.
22. Petrof, B. J., Shrager, J. B., Stedman, H. H., Kelly, A. M. and Sweeney, H. L. (1993) Dystrophin protects the sarcolemma from stresses developed during muscle contraction. *Proc. Natl. Acad. Sci. U S A* 90; 3710–3714.
23. Sahlin, K., Katz, A. and Henriksson, J. (1987) Redox state and lactate accumulation in human skeletal muscle during dynamic exercise. *Biochem. J.* 245; 551–556.
24. Saitoh, Y., Terada, N., Saitoh, S., Ohno, N., Fujii, Y. and Ohno, S. (2010) Histochemical approach of cryobiopsy for glycogen distribution in living mouse livers under fasting and local circulation loss conditions. *Histochem. Cell Biol.* 133; 229–239.
25. Saitoh, Y., Terada, N., Saitoh, S., Ohno, N., Jin, T. and Ohno, S. (2012) Histochemical analyses and quantum dot imaging of microvascular blood flow with pulmonary edema in living mouse lungs by "in vivo cryotechnique". *Histochem. Cell Biol.* 137; 137–151.
26. Saitoh, Y., Terada, N., Ohno, N., Hamano, A., Okumura, N., Jin, T., Saiki, I. and Ohno, S. (2014) Imaging of thrombosis and microcirculation in mouse lungs of initial melanoma metastasis with in vivo cryotechnique. *Microvasc. Res.* 91; 73–83.
27. Shi, L., Terada, N., Saitoh, Y., Saitoh, S. and Ohno, S. (2011) Immunohistochemical distribution of serum proteins in living mouse heart with in vivo cryotechnique. *Acta Histochem. Cytochem.* 44; 61–72.
28. Terada, N., Kato, Y., Fuji, Y., Ueda, H., Baba, T. and Ohno, S. (1998) Scanning electron microscopic study of flowing erythrocytes in hepatic sinusoids as revealed by 'in vivo cryotechnique'. *J. Electron Microsc. (Tokyo).* 47; 67–72.
29. Terada, N., Ohno, N., Ohguro, H., Li, Z. and Ohno, S. (2006) Immunohistochemical detection of phosphorylated rhodopsin in light-exposed retina of living mouse with in vivo cryotechnique. *J. Histochem. Cytochem.* 54; 479–486.
30. Wang, L. C. and Kernell, D. (2001) Fibre type regionalisation in lower hindlimb muscles of rabbit, rat and mouse: a comparative study. *J. Anat.* 199; 631–643.
31. Zhou, H., Ohno, N., Terada, N., Saitoh, S., Fujii, Y. and Ohno, S. (2007) Involvement of follicular basement membrane and vascular endothelium in blood follicle barrier formation of mice revealed by 'in vivo cryotechnique'. *Reproduction.* 134; 307–317.